Aerobic oxidation of 5-hydroxymethylfurfural to 2,5-diformylfuran on supported vanadium oxide catalysts: Structural effect and reaction mechanism*

Junfang Nie and Haichao Liu‡

National Laboratory for Molecular Sciences, State Key Laboratory for Structural Chemistry of Stable and Unstable Species, College of Chemistry and Molecular Engineering, Green Chemistry Center, Peking University, Beijing 100871, China

Abstract: The structure–activity relationship and reaction mechanism for selective oxidation of 5-hydroxymethylfurfural (HMF) to 2,5-diformylfuran (DFF) in toluene were studied on vanadium oxide domains on TiO_2, Al_2O_3, Nb_2O_5, ZrO_2, and MgO and with a wide range of VO_x surface densities. The structures of these catalysts were characterized by X-ray diffraction (XRD), diffuse reflectance UV–vis spectroscopy (UV–vis DRS), and Raman spectroscopy, and their reducibility was probed by H_2-temperature programmed reduction. The structures of the VO_x domains evolved from monovanadate to polyvanadate structures with increasing the VO_x surface densities, and finally to crystalline V_2O_5 clusters at surface densities above one-monolayer capacity. Within one-monolayer capacity, higher VO_x surface densities and more reducible supports led to higher reducibility and reactivity of the VO_x domains. The support surfaces covered with polyvanadates and V_2O_5 clusters and the supports with acidity favored the formation of DFF. The correlation between the reducibility and reactivity, together with the kinetic studies, suggests that the HMF oxidation to DFF proceeds via the redox mechanism involving the V^{5+}/V^{4+} redox cycles and the reoxidation of V^{4+} to V^{5+} by O_2 as the rate-determining step. These results may provide guidance for the design of more efficient catalysts for the HMF oxidation to synthesize DFF.

Keywords: biomass; heterogeneous catalysis; liquid phases; mechanism; structure–activity relationship; vanadium.

INTRODUCTION

It is known that the organic chemicals used at present are generally derived from fossil resources. However, as fossil resources are unrenewable and diminishing rapidly, it is of great interest to replace them with sustainable alternatives, such as biomass [1]. For example, the U.S. Department of Energy has predicted that 25 % of the chemicals will be produced from biomass by 2030 [2]. In this context, 5-hydroxymethylfurfural (HMF), as an important biomass-based platform molecule, has drawn increasing attention, and its reactions have been largely explored. In this work, we focus on selective oxidation of HMF to 2,5-diformylfuran (DFF), a versatile chemical intermediate for synthesis of Schiff bases [1], pharmaceuticals, and antifungal agents [3], as well as of polymers with various applications [4].

Traditionally, the synthesis of DFF from HMF oxidation involves the use of different oxidants including NaOCl [5], BaMnO$_4$ [6], oxalyl chloride, pyridinium chlorochromate, and trimethylammonium chlorochromate [7]. These oxidants are used in stoichiometric quantities, and many of them contain chlorine. They are clearly not green and will produce large amounts of wastes. In contrast, molecular oxygen is cheap and clean. Therefore, many efforts have been made to employ molecular oxygen as oxidant in this reaction on different homogeneous and heterogeneous catalysts. These catalysts include Co/Mn/Zr/Br, supported Pt, Mn(III)-salen, and V-based catalysts [5,8]. Among them, vanadium oxide (VO$_x$) catalysts are noticeable because of their heterogeneous nature and high selectivity to DFF. For example, Moreau and co-workers have reported an 85 % DFF yield (93 % selectivity at 91 % conversion) in toluene on V$_2$O$_5$/TiO$_2$ [8d]. However, in this preliminary report, systematic studies on the structures of the V$_2$O$_5$/TiO$_2$ catalysts and their performances are not presented, and the corresponding structural effects and reaction mechanism remain unclear. To address these issues, further studies therefore are necessary, which will be relevant to the tuning of the reaction pathways and of catalyst structures more efficient for the synthesis of DFF from the HMF oxidation.

Concerning the supported VO$_x$ catalysts, it is known that they have been widely used in various reactions, such as oxidative dehydrogenation of light alkanes [9], selective oxidation of methanol [10], and selective NO$_x$ reduction [11]. The VO$_x$ structures have been well characterized by X-ray diffraction (XRD), diffuse reflectance UV–vis spectroscopy (UV–vis DRS) and Raman spectroscopy, etc., demonstrating the structural evolution from isolated monovanadate to 2D polyvanadate domains and ultimately to crystalline V$_2$O$_5$ clusters with increasing VO$_x$ surface density [9,12]. These studies, although they are carried out mainly for gas-phase reactions on the VO$_x$ catalysts, will be beneficial to address the above-mentioned problems involved in the HMF oxidation in liquid phase.

Here, we present a detailed study of the HMF oxidation on the supported VO$_x$ catalysts with varying VO$_x$ surface densities. We examine the effects of the VO$_x$ surface densities and supports on the reducibility, activity, and selectivity of the active VO$_x$ domains. The supports include TiO$_2$, Al$_2$O$_3$, Nb$_2$O$_5$, ZrO$_2$, and MgO with a wide range of acid–base and redox properties. We characterize their structures and reducibilities by XRD, Raman, UV–vis DRS, and H$_2$-temperature-programmed reduction (H$_2$-TPR). We also examine the effects of reaction parameters and the mechanism for the HMF oxidation.

EXPERIMENTAL

Catalyst preparation

Supported VO$_x$ catalysts were prepared by incipient wetness impregnation of TiO$_2$ (Alfa Asear, S_{BET} = 128 m^2/g), Al$_2$O$_3$ (Sigma Aldrich, S_{BET} = 175 m^2/g), Nb$_2$O$_5$ (prepared according to Ouqour et al. [13], S_{BET} = 48 m^2/g), ZrO$_2$ (prepared according to Li et al. [14], S_{BET} = 179 m^2/g), and MgO (prepared according to Guan et al. [15], S_{BET} = 101 m^2/g) with an aqueous solution of ammonium metavanadate (NH$_4$VO$_3$; Beijing Chemicals, AR grade) and oxalic acid (H$_2$C$_2$O$_4$; Beijing Chemicals, AR grade). The V contents were varied by changing the NH$_4$VO$_3$ concentrations in the impregnating solutions. The impregnated samples were dried at 383 K in ambient air overnight, and then treated in flowing dry air at 773 K for 4 h.

Catalyst characterization

Brunauer–Emmett–Teller (BET) surface areas were measured by nitrogen adsorption at 78.3 K on a Micromeritics ASAP 2010 analyzer. Prior to the measurements, the samples were degassed at 433 K for 2 h under dynamic vacuum conditions.

XRD patterns were obtained on a Rigaku D/Max-2000 diffractometer from 20 to 80º at a scanning rate of 4º min^{-1} using a Cu Kα radiation (λ = 1.5406 Å) source. The applied voltage and current were 40 kV and 100 mA, respectively.

X-ray photoelectron spectra were measured on an AXIS Ultra (Kratos, UK) spectrometer with an Al anode (Al Kα, hv = 1486.6 eV), operated at 225 W. The binding energies were calibrated by using the C1s line at 248.8 eV as reference.

Raman spectra were collected in the range 200–1100 cm^{-1} on a Horiba HR800 Raman spectrometer using a He–Ne laser at a wavelength of 514 nm. The resolution was better than 1 cm^{-1}, and the laser power was set to 10 mW. The Raman spectra were taken after sample powders were treated in a quartz cell at 673 K in flowing dry air for 1 h and then cooled to room temperature.

UV–vis DRS spectra were recorded on a Perkin 650S spectrophotometer equipped with an integration sphere diffuse reflectance attachment. The samples were pressed into self-supported disks of 1 mm in thickness, and then placed in a quartz reaction cell and treated in flowing dry air at 723 K for 1 h. After being cooled to room temperature, UV–vis DRS spectra were taken in the range 200–800 nm using $BaSO_4$ as a reference compound. The Kubelka–Munk function $F(R_\infty)$ was used to convert reflectance data into absorption spectra, and the edge energy (E_g) was estimated from the intercept of the straight line in the low-energy rise of the plot of $[F(R_\infty)hv]^2$ as a function of hv, where hv is the incident photon energy [9b,c].

H_2-TPR experiments were performed on a flow unit (TP5000, Tianjin Xianquan). Catalysts containing approximately 2 mg of V were placed in a quartz cell, and heated in a 5 % H_2/N_2 flow at a rate of 30 cm^3/min (Beijing Huayuan, certified mixture). The temperature was ramped from 298 to 1023 K at a rate of 10 K/min. The H_2 consumption was quantified by integration of the corresponding TCD signals calibrated by the reduction of CuO powder in the identical conditions. The initial VO_x reduction temperatures for the catalysts, referred to as T_{onset}, were set to the temperatures at which 10 % of the VO_x species was reduced.

Catalytic HMF oxidation reactions

Selective oxidation of HMF was carried out in a 100-ml Teflon-lined stainless steel autoclave equipped with a condenser and mechanical stirring bar. In a typical run, 50 ml toluene containing 1 mmol HMF and 126 mg of catalysts was introduced to the autoclave. Afterwards, the autoclave was sealed, fully flushed with air, and then rapidly heated to reaction temperatures. The temperatures remained constant during the reactions. The stirring speed was kept at 800 rpm to ensure there was no influence of mass transfer on reactions. Reactants and products were analyzed by HPLC (Shimadzu LC-20A) using a UV detector and an Alltech OA-1000 organic acid column (analysis conditions: mobile phase 0.005 M H_2SO_4, flow rate 0.7 ml/min, oven temperature 353 K). Reaction activities were reported as molar HMF conversion rates per mole of V atoms per hour, and DFF selectivities were calculated on a carbon basis.

After the reaction was stopped and the supported VO_x catalysts were removed, the reaction solutions were measured by inductively coupled plasma-atomic emission spectroscopy (ICP-AES), showing that V content in the filtrates was below the detection limit (<0.1 %). Meanwhile, once the catalysts were removed from the reaction systems, the HMF oxidation reactions stopped. These experiments confirmed the heterogeneous nature of the HMF oxidation on the supported VO_x catalysts under the reaction conditions employed in this work.

RESULTS AND DISCUSSION

Figure 1 shows activities (normalized per V atom) and DFF selectivities at 363 K and 1.6 MPa air on VO_x/TiO_2 and VO_x/Al_2O_3 catalysts as a function of VO_x surface density. The VO_x surface densities (V/nm^2) were calculated from V contents and surface areas, as listed in Table 1. The activities and

selectivities were compared at similar HMF conversions (~30 %). On VO_x/TiO_2, the activities increased with increasing the VO_x surface densities, and reached a maximum value of 24.4 h^{-1} at 3.0 V/nm^2 (Fig. 1a). Further increasing the VO_x surface densities to 41.8 V/nm^2 led to a sharp decline in the activities. The DFF selectivities increased from 58.1 to 69.2 % with increasing the VO_x surface densities from 0.6 to 3.0 V/nm^2, which then remained essentially constant at higher surface densities between 3.0–41.8 V/nm^2 (Fig. 1a). These constant DFF selectivities did not change even at >90 % HMF conversions (Fig. 2), showing that DFF was stable on the VO_x catalysts under the conditions employed in
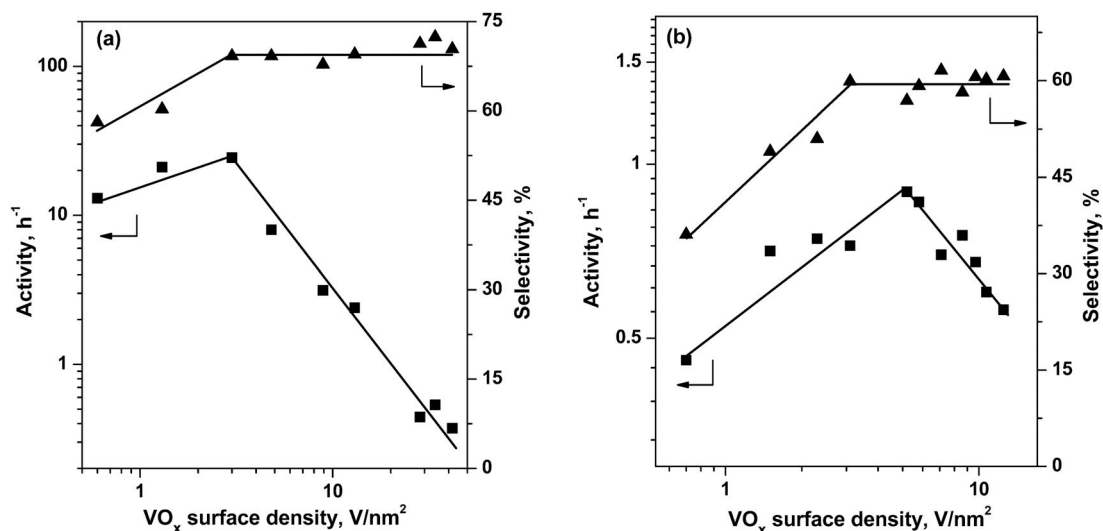

Fig. 1 Dependence of activities and selectivities on VO_x surface densities for (a) VO_x/TiO_2 and (b) VO_x/Al_2O_3 catalysts (363 K, 1.6 MPa air, 1 mmol HMF, 126 mg catalyst, 50 ml toluene, ~30 % HMF conversion).
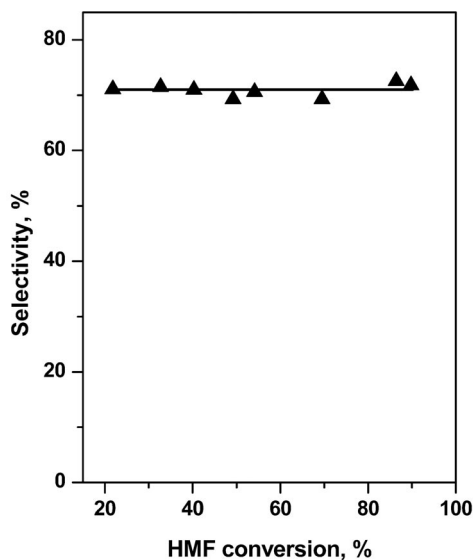

Fig. 2 Dependence of DFF selectivities on HMF conversions for 3.6 wt % VO_x/TiO_2 catalyst (363 K, 1.6 MPa air, 1 mmol HMF, 126 mg catalyst, 50 ml toluene, 0.2–4 h).

this work. Similar effects of the VO_x surface densities were observed with the VO_x/Al_2O_3 catalysts (Fig. 1b). Their activities reached the maximum value of 0.90 h^{-1} at 5.8 V/nm^2 by increasing the surface densities in the whole range of 0.7–15.5 V/nm^2. Their DFF selectivities increased monotonically to the constant value of ~59 % for the surface densities higher than 3.1 V/nm^2. These observed changes are closely relevant to the structural changes of the VO_x/TiO_2 and VO_x/Al_2O_3 catalysts, as shown below.

Table 1 BET surface areas, nominal VO_x surface densities and, initial reduction temperatures (T_{onset}) for VO_x/TiO_2 and VO_x/Al_2O_3 catalysts.

Catalyst	Surface area (m^2/g)	VO_x surface density (V/nm^2)	T_{onset} (K)
1.0 wt % VO_x/Al_2O_3	164	0.7	730
2.0 wt % VO_x/Al_2O_3	156	1.5	707
3.0 wt % VO_x/Al_2O_3	154	2.3	699
4.0 wt % VO_x/Al_2O_3	148	3.1	677
6.0 wt % VO_x/Al_2O_3	134	5.2	675
7.0 wt % VO_x/Al_2O_3	139	5.8	676
8.0 wt % VO_x/Al_2O_3	130	7.1	676
9.0 wt % VO_x/Al_2O_3	122	8.6	680
10.0 wt % VO_x/Al_2O_3	119	9.7	682
12.0 wt % VO_x/Al_2O_3	111	12.5	688
14.0 wt % VO_x/Al_2O_3	104	15.5	703
0.6 wt % VO_x/TiO_2	129	0.6	669
1.3 wt % VO_x/TiO_2	121	1.3	666
2.6 wt % VO_x/TiO_2	103	3.0	657
3.6 wt % VO_x/TiO_2	88	4.8	662
5.1 wt % VO_x/TiO_2	68	8.9	676
6.6 wt % VO_x/TiO_2	59	13.0	694
7.2 wt % VO_x/TiO_2	31	28.4	729
9.9 wt % VO_x/TiO_2	34	34.0	738
12.2 wt % VO_x/TiO_2	34	41.8	744

Figure 3 shows XRD patterns for the VO_x/TiO_2 and VO_x/Al_2O_3 catalysts. Only diffraction peaks of anatase TiO_2 and Al_2O_3 phases were present for the VO_x surface densities lower than ~8.0 V/nm^2, the theoretical coverage of a polyvanadate monolayer [9b,12a]. Crystalline V_2O_5 was detected on VO_x/TiO_2 as the VO_x surface densities exceeded 8.9 V/nm^2, and on VO_x/Al_2O_3 at 8.6 V/nm^2. Raman spectra confirmed these results.

As shown in Fig. 4a, in the range 750–1100 cm^{-1} (for brevity, the Raman bands below 750 cm^{-1} due to supports are not shown), dehydrated VO_x species on TiO_2 with 0.6 V/nm^2 exhibited a Raman band at 1028 cm^{-1}, which corresponds to the V=O stretching mode in isolated monovanadate structure [9b,12b]. This peak shifted slightly to 1032 cm^{-1} for 8.9 V/nm^2, indicating the transformation of the isolated monovanadate species to polyvanadate species with increasing the VO_x surface densities [12b,c]. Along with such shift, a broad band around 920 cm^{-1} appeared on the samples with the VO_x surface densities higher than 1.3 V/nm^2. This feature is ascribed to V–O–V stretches in the 2D polyvanadate species [12b,c]. The Raman band at 995 cm^{-1}, characteristic of crystalline V_2O_5 [12b], was detected as the VO_x surface densities exceeded 8.9 V/nm^2, in accordance with the XRD results (Fig. 3a). The VO_x/Al_2O_3 catalysts exhibited similar changes in the Raman features (in the range 750–1100 cm^{-1}) with the VO_x surface densities. As shown in Fig. 4b, the Raman band appeared at 1012 cm^{-1}, characteristic of the terminal V=O bond in the isolated monovanadate species [12a], which also shifted to higher frequencies as the 2D polyvanadate species were formed with increasing the VO_x surface densities. This is accompanied by the appearance of the broad Raman feature around 920 cm^{-1},
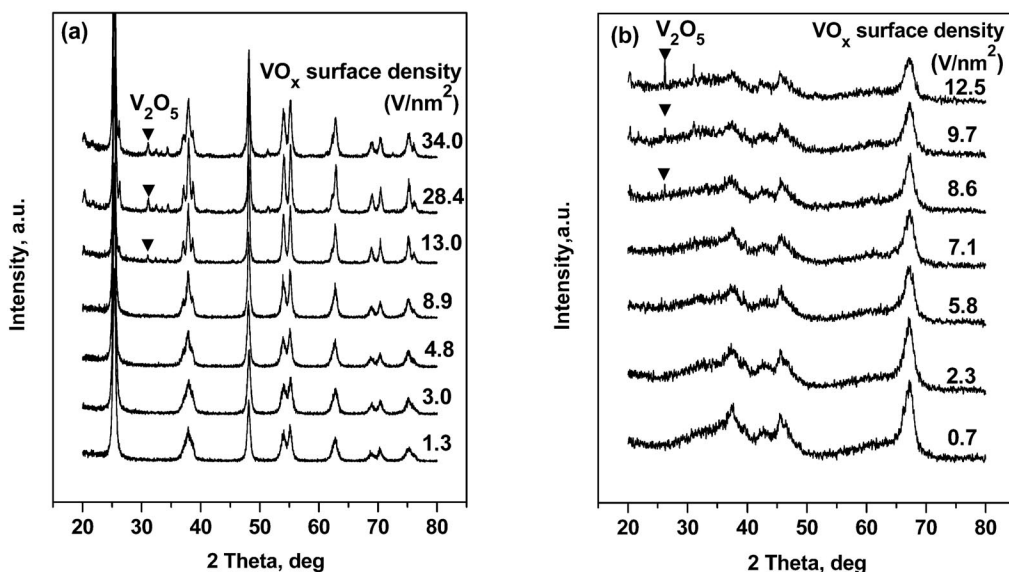
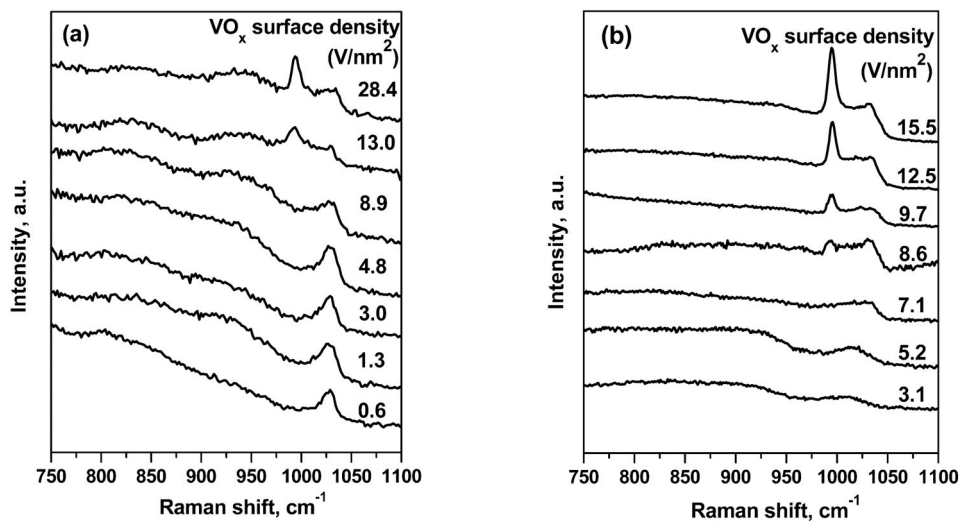**Fig. 3** XRD patterns for (a) VO_x/TiO_2 and (b) VO_x/Al_2O_3 with various VO_x surface densities.

Fig. 4 Raman spectra of (a) VO_x/TiO_2 and (b) VO_x/Al_2O_3 under dehydrated conditions at 298 K after treatment in flowing dry air at 673 K for 1 h.

arising from the V–O–V stretches in the distorted polyvanadates [12b,c]. Further increasing the VO_x surface densities to above 8.6 V/nm^2 led to the appearance of the band at 995 cm^{-1}, owing to the formation of crystalline V_2O_5 [9b,12c].

Such structural changes for the supported VO_x catalysts can be further characterized by UV–vis DRS, which is effective to probe the coordination state of the V cations because the energy required for O^{2-} to V^{5+} charge transfer is sensitive to the local structures of the V cations [9b,12c]. As TiO_2 possesses strong UV–vis DRS absorption, which overlaps with the spectra of the VO_x species, the UV–vis DRS spectra were only recorded for the VO_x/Al_2O_3 catalysts. Considering the charge-transfer band is

generally broad, it is more useful to use the energy at the absorption edge (E_g) to probe the charge-transfer transition. Figure 5 shows the corresponding E_g values of the VO_x species. The E_g was above 2.6 eV at 0.7 V/nm^2 and declined sharply as the surface densities approached 3.1 V/nm^2, indicating a predominance of the isolated monovanadate species at lower surface densities [12c]. Further increasing the VO_x surface densities led to an increase of the polyvanadate species, as indicated by the continuous decline in the E_g. Finally, the E_g tended to approach the value typical of crystalline V_2O_5 (~2 eV) [12c].
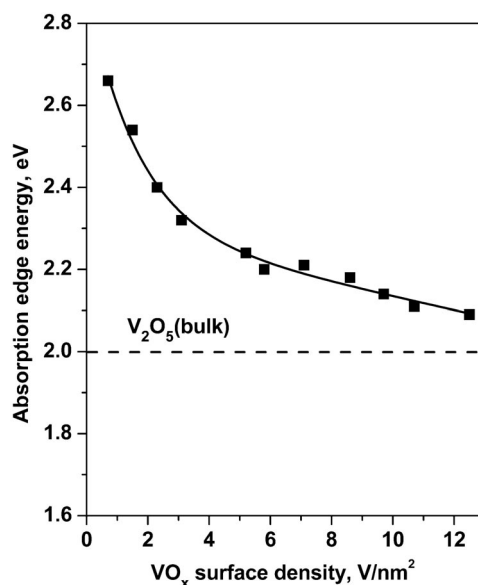

Fig. 5 Dependence of the UV–vis absorption edge energies on the VO_x surface densities for VO_x/Al_2O_3 at 298 K after dehydration treatment in flowing dry air at 723 K for 1 h.

In summary, the structures of the VO_x species supported on TiO_2 and Al_2O_3 evolve from the isolated monovanadate to the 2D polyvanadate structures at the VO_x surface densities below one-monolayer capacity (i.e., 8.9 and 8.6 V/nm^2, respectively), and then to the bulk V_2O_5 clusters at high surface densities, as reported extensively in the literature [9–12]. By referring to these structural changes, we can understand the VO_x surface density effects on the HMF oxidation shown in Fig. 1. The observed increase in the DFF selectivities to the constant values with increasing the surface densities reveals that the support surfaces covered with the polyvanadates and V_2O_5 clusters, relative to the isolated monovanadates, favor the high DFF selectivities on VO_x/TiO_2 and VO_x/Al_2O_3, consistent with the finding by Moreau et al. [8d].

In terms of the observed effects of the VO_x surface density and structure on the reaction activities (Fig. 1), from the structural characterization of the VO_x species, it is known that the VO_x species at the surface densities below one monolayer capacity (approximately 8–9 V/nm^2) are dispersed well on TiO_2 and Al_2O_3, and nearly all of them are exposed and accessible to the reactants. Therefore, the activities per V atom for these catalysts reflect the intrinsic reactivity of the exposed VO_x species. Clearly, the observed change in the activities with the VO_x surface densities below 8–9 V/nm^2 is not caused by the change in the accessibilities of the VO_x species, but by the change in their intrinsic reactivity. At a given VO_x surface density (below 8–9 V/nm^2), the higher activities for VO_x species on TiO_2 than on Al_2O_3 reflect their higher intrinsic reactivity on TiO_2. Such change in their reactivity is consistent with their difference in reducibility, as discussed below. Above 8–9 V/nm^2, crystalline V_2O_5 phases formed and coexisted with the dispersed VO_x species, i.e., monovanadates and polyvanadates (Figs. 3–5). The

observed decrease in the activities with increasing the VO_x surface densities may be caused by either the lower intrinsic reactivity of the VO_x domains or their lower accessibilities. Therefore, only for the samples with the surface densities below 8–9 V/nm^2, their intrinsic reactivity and reducibility can be used to rigorously understand the genesis of the effect of the surface density and structure.

The reducibility for the VO_x catalysts supported on TiO_2 and Al_2O_3 was probed by H_2-TPR. As shown in Fig. 6a, the VO_x/TiO_2 samples exhibited only one reduction peak, which shifted from 727 to 843 K as the VO_x surface densities increased from 0.6 to 41.8 V/nm^2, showing the similar trend reported in the literature [16]. Differently, the reduction peak for VO_x/Al_2O_3 (Fig. 6b) shifted from 812 to 757 K with increasing the VO_x surface densities from 0.7 to 5.8–7.1 V/nm^2, and then back to higher temperatures by further increasing the surface densities. However, although the peak temperature is frequently used to probe the reducibility, the initial reduction stage is most relevant to the redox cycles required in selective oxidation reactions of different hydrocarbons and alcohols on VO_x and MoO_x catalysts, etc. [17,18], owing to the fact that few reduced V^{4+}, Mo^{4+}, or other metal centers are present with a formation of a low surface density of oxygen vacancies during the steady-state catalysis. Therefore, we here use the initial reduction temperatures (T_{onset}) to estimate and compare the reducibility for different catalysts (Table 1). For the VO_x surface densities below 8–9 V/nm^2, the T_{onset} for VO_x/TiO_2 decreased with increasing the VO_x surface densities, and reached a lowest value of 657 K at 3.0 V/nm^2; then the T_{onset} increased by further increasing the surface densities. A similar trend was found on VO_x/Al_2O_3, which exhibited a minimum T_{onset} of 675 K at 5.2 V/nm^2 (Table 1). By comparing the T_{onset} values with the reaction activities for the VO_x/TiO_2 and VO_x/Al_2O_3 catalysts, we can find a close correlation between them. The activities for VO_x/TiO_2 increased from 13.0 to 24.4 h^{-1} as T_{onset} decreased from 669 to 657 K with increasing the VO_x surface densities from 0.6 to 3.0 V/nm^2. Further increasing the surface densities to 8.9 V/nm^2 led to the shift of the T_{onset} to 676 K and accordingly the decline in the activity to 3.1 h^{-1}. For VO_x/Al_2O_3, the activities increased from 0.46 to 0.90 h^{-1} as T_{onset} decreased from 730 to 675 K with increasing the VO_x surface densities from 0.7 to 5.2 V/nm^2, followed by the concurrent increase in the T_{onset} values and the decrease in the activities at the higher surface densities.
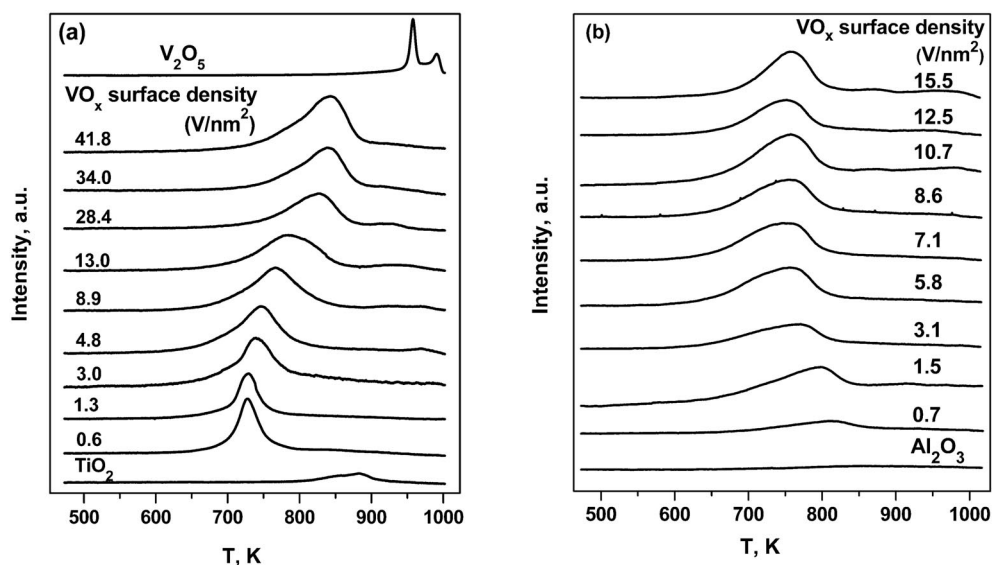

Fig. 6 H_2-TPR profiles for (a) VO_x/TiO_2 and (b) VO_x/Al_2O_3 catalysts with varying VO_x surface densities.

To verify this correlation between activity and T_{onset}, the VO_x species supported on the other three oxides, ZrO_2, Nb_2O_5, and MgO, were also examined at about one-monolayer VO_x coverage (Table 2). As shown in Table 2, the T_{onset} decreased by ~100 K as the support changed from MgO, Nb_2O_5, Al_2O_3, and TiO_2 to ZrO_2 with different surface acid-basicity and redox property. In parallel with this trend, the activities increased almost linearly from 0.49 to 1.3 h^{-1}, except for VO_x/TiO_2. The specialty of the TiO_2 support, relative to other supports examined here, is still being investigated. Moreover, supports also influence the DFF selectivities on the VO_x catalysts. More acidic Nb_2O_5, relative to more basic MgO, favored higher DFF selectivity (72.0 vs. 42.1 %), most likely due to their acid-basicity effects on the adsorption and desorption of HMF and DFF, etc. Such support effects accord with the general findings with the supported VO_x, MoO_x, and other metal oxide catalysts that more reducible supports lead to higher reducibility of the active metal oxide domains and their higher reactivity, while the acidic nature of the supports favors the formation of the target products [17a,18].

Table 2 HMF oxidation activities, DFF selectivities, and initial reduction temperatures (T_{onset}) of different oxide-supported VO_x catalysts with one-monolayer VO_x coverage.

Catalyst	VO_x surface density (V/nm^2)	T_{onset} (K)	Activity (h^{-1})	Selectivity (%)
5.1 wt % VO_x/TiO_2	8.9	676	3.15	69.6
8.0 wt % VO_x/ZrO_2	6.8	647	1.27	70.3
9.0 wt % VO_x/Al_2O_3	8.6	680	0.75	58.2
3.0 wt % VO_x/Nb_2O_5	9.2	722	0.63	72.0
5.5 wt % VO_x/MgO	8.6	751	0.49	42.1

Reaction conditions: 363 K, 1.6 MPa air, 1 mmol HMF, 126 mg catalyst, 50 ml toluene, ~30 % HMF conversion.

Such correlation between the reducibility and reactivity reflects the involvement of the Mars–van Krevelene redox mechanism, using surface lattice oxygen atoms of the VO_x domains in the HMF oxidation to DFF. The involvement of lattice oxygen atoms was confirmed by anaerobic oxidation of HMF. The anaerobic experiment was conducted on VO_x/TiO_2 (9.9 wt %, 34.0 V/nm^2) under N_2 atmosphere at 363 K and 1.6 MPa N_2. The initial activity was obtained after the reaction in N_2 for 5 min, and it was comparable to the activity in air (0.50 vs. 0.73 h^{-1}). The DFF selectivities were also similar (71.2 vs. 70.6 %) in N_2 and air. These results are consistent with the involvement of lattice oxygen in the HMF conversion to DFF, which, based on the following X-ray photoelectron spectroscopy (XPS) data, appears to proceed via V^{5+}/V^{4+} redox cycles during the aerobic catalysis. Such a redox process is depicted in Scheme 1, including the HMF oxidation to DFF with the lattice oxygen atoms on the VO_x domains, leading to the reduction of V^{5+} to V^{4+}, followed by the replenishment of the consumed lattice oxygen atoms (i.e., oxygen vacancies) with gaseous O_2, leading to the reoxidation of V^{4+} to V^{5+}. The formation of the reduced V^{4+} centers was detected by XPS on VO_x/TiO_2, showing an apparent increase in the V^{4+} faction to 16.4 % after the aerobic oxidation of HMF from 3.8 % for the fresh catalyst
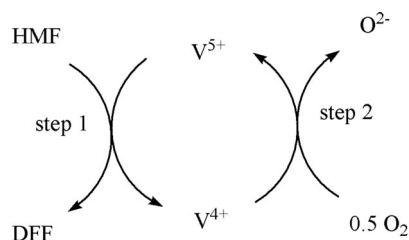
Scheme 1 Proposed reaction mechanism involving V^{5+}/V^{4+} redox cycles.

(Table 3). Such increase in the surface V^{4+} concentration after the oxidation catalysis implies that the second reoxidation step might be slow and limit the overall rate for the HMF oxidation to DFF. This is consistent with the effects of air pressures and HMF concentrations.

Table 3 XPS results of fresh and used VO_x/TiO_2 catalysts for HMF oxidation.

Catalyst	Binding energy of V $2p_{3/2}$ (eV)		Relative amount (%)	
	V^{5+}	V^{4+}	V^{5+}	V^{4+}
Fresh	517.6	516.1	96.2	3.8
Used[a]	517.5	516.3	83.6	16.4

[a]Reaction conditions: 9.9 wt % VO_x/TiO_2, 363 K, 1.6 MPa air, 1 mmol HMF, 126 mg catalyst, 50 ml toluene, 2 h.

Figure 7 shows the effect of the air pressures on the activities and DFF selectivities at similar HMF conversion (~30 %) on 3.6 wt % VO_x/TiO_2 (4.8 V/nm^2). The activities increased linearly as the air pressure increased from 0.1 to 0.8 MPa, and then tended to level off and approach saturation values by increasing the air pressure to above 1.5 MPa. Such an effect is not due to the effect on the O_2 concentrations and thus on the mass transfer of O_2 in the liquid phase, based on our estimation of the O_2 transport rate in the reaction conditions employed. Therefore, the oxygen pressure effect agrees with the proposition that the reoxidation of V^{4+} to V^{5+} is slow and might be the rate-determining step in the HMF oxidation to DFF. The O_2 pressure also influences the DFF selectivities. They increased from 62.3 to 71.3 % as the air pressure increased from 0.1 to 0.4 MPa, and then decreased slightly to 66.2 % at 2.4 MPa.
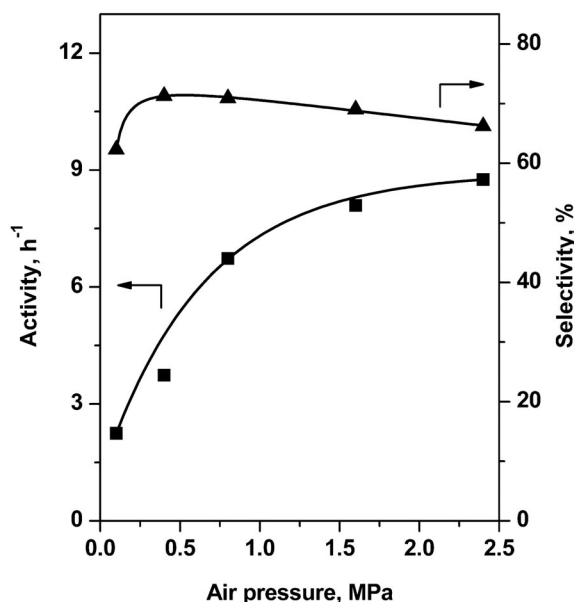

Fig. 7 Effects of air pressure on HMF oxidation activities and DFF selectivities on 3.6 wt % VO_x/TiO_2 (4.8 V/nm^2, 1 mmol HMF, 363 K, 126 mg catalyst, 50 ml toluene, ~30 % HMF conversion).

The activities and DFF selectivities were less sensitive to the variation of the HMF concentrations. As shown in Fig. 8, at low HMF concentrations, their slight increase from 6.6 to 10.0 mmol/L led to a sharp increase in the activities. Then the activities remained unaffected by further increasing the HMF concentrations in a wide range (10.0–40.0 mmol/L). The DFF selectivities decreased slightly to constant values as the HMF concentrations increased from 6.6 to 10.0 mmol/L. These results indicate that HMF readily adsorb on the VO_x/TiO_2 surface, and thus reach the saturation coverage.

We have also explored the effect of the reaction temperature on the HMF oxidation activitities and DFF selectivities on 3.6 wt % VO_x/TiO_2. As shown in Fig. 9, the HMF oxidation occurred at 323 K, but with a low activity (0.67 h^{-1}), which increased exponentially to 85.9 h^{-1} with increasing the reaction temperature to 403 K. The activation energy was also accordingly estimated to be 67 kJ/mol, similar to the value (77 kJ/mol) reported in the literature [8d]. The DFF selectivities increased with increasing the temperature, and reached the maximum value of 70.2 % at 363 K.
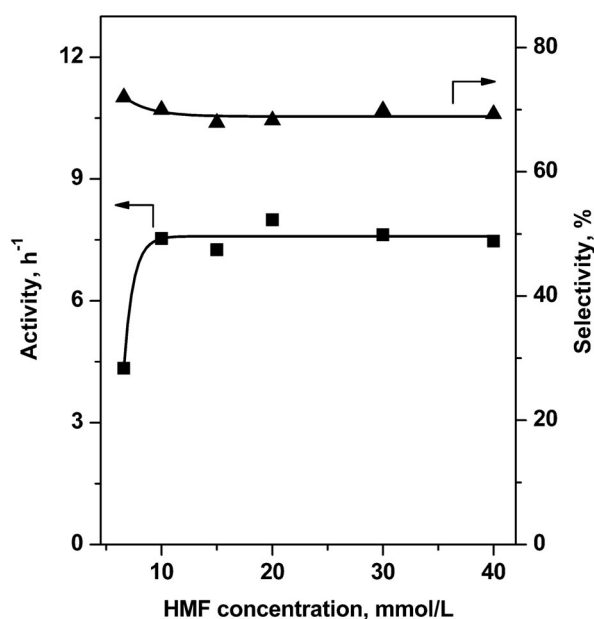

Fig. 8 Effects of HMF concentration on HMF oxidation activities and DFF selectivities on 3.6 wt % VO_x/TiO_2 (4.8 V/nm^2, 363 K, 1.6 MPa air, 126 mg catalyst, 50 ml toluene, keeping a constant consumption of HMF).
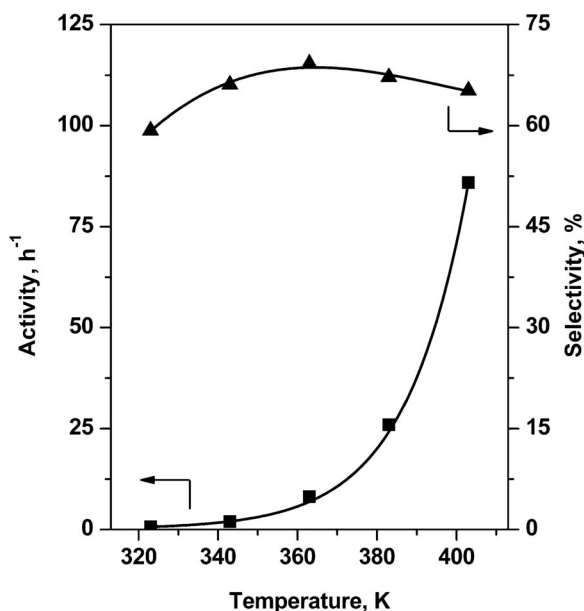
Fig. 9 Effects of reaction temperature on HMF oxidation activities and DFF selectivities on 3.6 wt % VO_x/TiO_2 (4.8 V/nm^2, 1 mmol HMF, 1.6 MPa air, 21–126 mg catalyst, 50 ml toluene, ~30 % HMF conversion).

CONCLUSION

VO_x domains supported on TiO_2, Al_2O_3, Nb_2O_5, ZrO_2, and MgO catalyze the selective oxidation of HMF to DFF. The VO_x surface densities and supports influence the VO_x structures and reducibility as well as their catalytic properties. The VO_x structures evolve from isolated monovanadate to 2D poly-vanadate domains with increasing the VO_x surface densities within one monolayer capacity, and then to crystalline V_2O_5 clusters at the high surface densities. Such structural change with the VO_x surface densities within one monolayer capacity lead to a parallel increase in the reducibility of the VO_x domains and their intrinsic activities. More reducible TiO_2 and ZrO_2 supports lead to more reducible and reactive VO_x domains. The support surfaces covered with polyvanadates and V_2O_5 clusters and the supports with acidity favor the formation of DFF. The HMF oxidation to DFF appears to proceed via the redox mechanism involving the V^{5+}/V^{4+} redox cycles and the reoxidation of V^{4+} to V^{5+} by O_2 as the rate-determining step.

ACKNOWLEDGMENTS

REFERENCES

1. A. Corma, S. Iborra, A. Velty. *Chem. Rev.* **107**, 2411 (2007).
2. J. N. Chheda, G. W. Huber, J. A. Dumesic. *Angew. Chem., Int. Ed.* **46**, 7164 (2007).
3. (a) K. T. Hopkins, W. D. Wilson, B. C. Bender, D. R. McCurdy, J. E. Hall, R. R. Tidwell, A. Kumar, M. Bajic, D. W. Boykin. *J. Med. Chem.* **41**, 3872 (1998); (b) M. Del Poeta, W. A. Schell, C. C. Dykstra, S. Jones, R. R. Tidwell, A. Czarny, M. Bajic, M. Bajic, A. Kumar, D. Boykin, J. R. Perfect. *Antimicrob. Agents Chemother.* **42**, 2495 (1998).
4. (a) A. Gandini, N. M. Belgacem. *Polym. Int.* **47**, 267 (1998); (b) A. S. Amarasekara, D. Green, L. D. Williams. *Eur. Polym. J.* **45**, 595 (2009).
5. A. S. Amarasekara, D. Green, E. McMillan. *Catal. Commun.* **9**, 286 (2008).
6. F. W. Lichtenthaler. *Acc. Chem. Res.* **35**, 728 (2002).
7. J. Lewkowski. *Arkivoc* **1**, 17 (2001).
8. (a) J. Ma, Z. Du, J. Xu, Q. Chu, Y. Pang. *ChemSusChem* **4**, 51 (2011); (b) O. C. Navarro, A. C. Canos, S. I. Chornet. *Top. Catal.* **52**, 304 (2009); (c) C. Carlini, P. Patrono, A. M. R. Galletti, G. Sbrana, V. Zima. *Appl. Catal., A* **289**, 197 (2005); (d) C. Moreau, R. Durand, C. Pourcheron, D. Tichit. *Stud. Surf. Sci. Catal.* **108**, 399 (1997).
9. (a) H. H. Kung. *Adv. Catal.* **40**, 1 (1994); (b) A. Khodakov, J. Yang, S. Su, E. Iglesia, A. T. Bell. *J. Catal.* **177**, 343 (1998); (c) H. Tian, E. I. Ross, I. E. Wachs. *J. Phys. Chem. B* **110**, 9593 (2006).
10. B. M. Weckhuysen, D. E. Keller. *Catal. Today* **78**, 25 (2003).
11. G. T. Went, L.-J. Leu, R. R. Rosin, A. T. Bell. *J. Catal.* **134**, 492 (1992).
12. (a) I. E. Wachs. *Catal. Today* **27**, 437 (1996); (b) J.-M. Jehng, G. Deo, B. M. Weckhuysen, I. E. Wachs. *J. Mol. Catal., A* **110**, 41 (1996); (c) B. Kilos, A. T. Bell, E. Iglesia. *J. Phys. Chem. C* **113**, 2830 (2009).
13. A. Ouqour, G. Coudurier, J. C. Vedrine. *J. Chem. Soc., Faraday Trans.* **89**, 3151 (1993).
14. W. Li, H. Huang, H. Li, W. Zhang, H. Liu. *Langmuir* **24**, 8358 (2008).
15. H. Guan, P. Wang, H. Wang, B. Zhao, Y. Zhu, Y. Xie. *Acta Phys. Chim. Sin.* **22**, 804 (2006).
16. I. Giakoumelou, C. Fountzoula, C. Kordulis, S. Boghosian. *J. Catal.* **239**, 1 (2006).
17. (a) K. Chen, A. T. Bell, E. Iglesia. *J. Catal.* **209**, 35 (2002); (b) K. Chen, S. Xie, A. T. Bell, E. Iglesia. *J. Catal.* **198**, 232 (2001).
18. (a) H. Liu, P. Cheung, E. Iglesia. *J. Catal.* **217**, 222 (2003); (b) H. Liu, E. Iglesia. *J. Phys. Chem. B* **109**, 2155 (2005).